





Modeling Boron–Oxygen Degradation and Self-Repairing Silicon PV Modules in the Field

Alison M. Ciesla , Jose I. Bilbao , Catherine E. Chan , David N. R. Payne, Daniel Chen , Moonyong Kim , Stuart R. Wenham, and Brett J. Hallam 

I. INTRODUCTION

Abstract—Photovoltaic (PV) cells manufactured using p-type Czochralski wafers can degrade significantly in the field due to boron–oxygen (BO) defects. Commercial hydrogenation processes can now passivate such defects; however, this passivation can be destabilized under certain conditions. Module operating temperatures are rarely considered in defect studies, and yet are critical to understanding the degradation and passivation destabilization that may occur in the field. Here we show that the module operating temperatures are highly dependent on location and mounting, and the impact this has on BO defects in the field. The System Advisor Model is fed with typical meteorological year data from four locations around the world (Hamburg, Sydney, Tucson, and Wuhan) to predict module operating temperatures. We investigate three PV system mounting types: building integrated (BIPV), rack-mounted rooftop, and rack mounted on flat ground for a centralized system. BO defect reactions are then simulated, using a three-state model based on experimental values published in the literature and the predicted module operating temperatures. The simulation shows that the BIPV module in Tucson reaches 94 °C and stays above 50 °C for over 1600 h per year. These conditions could destabilize over one-third of passivated BO defects, resulting in a 0.4% absolute efficiency loss for the modules in this work. This absolute efficiency loss could be double for higher efficiency solar cell structures, and modules. On the other hand, passivation of BO defects can occur in the field if hydrogen is present and the module is under the right environmental conditions. It is therefore important to consider the specific installation location and type (or predicted operating temperatures) to determine the best way to treat BO defects. Modules that experience such extreme sustained conditions should be manufactured to ensure incorporation of hydrogen to enable passivation of BO defects in the field, thereby enabling a “self-repairing module.”

Index Terms—Boron–oxygen defects, destabilization, hydrogen passivation, module operating temperature, self-repairing module.

Manuscript received April 5, 2019; revised July 19, 2019 and September 24, 2019; accepted September 25, 2019. Date of publication October 24, 2019; date of current version December 23, 2019. This work was supported by the Australian Government through the Global Innovation Linkages program – project GIL53868. (Corresponding author: Alison M. Ciesla.)

A. M. Ciesla, J. I. Bilbao, C. E. Chan, D. Chen, M. Kim, S. R. Wenham, and B. J. Hallam are with the School of Photovoltaic and Renewable Energy Engineering, UNSW Sydney, Kensington, NSW 2052, Australia (e-mail: a.ciesla@unsw.edu.au; j.bilbao@unsw.edu.au; catherine.chan@unsw.edu.au; david.payne@mq.edu.au; moonyong.kim@unsw.edu.au; s.wenham@unsw.edu.au; brett.hallam@unsw.edu.au).

D. N. R. Payne is with the School of Engineering, Macquarie University, Macquarie Park, NSW 2113, Australia (e-mail: d.n.payne@unsw.edu.au).

Color versions of one or more of the figures in this article are available online at <http://ieeexplore.ieee.org>.

Digital Object Identifier 10.1109/JPHOTOV.2019.2945161

THE PHOTOVOLTAIC (PV) industry is dominated by crystalline silicon solar cells and modules, and of these, approximately 40% of worldwide production uses boron-doped Czochralski (Cz) grown substrates [1]. However, such substrates, and the solar cells fabricated on them, are subject to a degradation in performance when exposed to illumination [2]–[5]. This degradation, caused by boron–oxygen (BO) defects, is often referred to as “light-induced degradation”; however, defect formation can also occur in the dark in the presence of carrier injection. Hence, it is actually a carrier-induced degradation (CID) mechanism [5], [6]. Due to the existence of many forms of carrier- or light-induced degradation, a less ambiguous terminology to refer to this degradation is BO degradation, or BO-related CID (BO-CID) [7].

While the specific structure and formation process for the defect are still under debate [7], it is widely accepted that the defect consists of a complex of boron and interstitial oxygen, namely, a BO defect [4], [8]–[11]. The magnitude of degradation has been correlated linearly with the concentration of boron dopants (in purely boron-doped material) and quadratically with the interstitial oxygen concentration in the silicon [4], [12]; in compensated silicon the net doping is more relevant than the boron concentration [13]. Hence, the degradation is heavily dependent on the impurity concentrations in the incoming silicon wafer.

For conventional screen-printed solar cells with a full area aluminum back-surface-field (Al-BSF), efficiency losses are typically 3–4% relative [14]. However, the percentage of degradation also depends on the solar cell structure. High-efficiency solar cell structures such as the passivated emitter and rear cell (PERC), have a stronger dependence on the bulk lifetime within the silicon and are therefore prone to larger potential efficiency losses due to CID [15]. For PERC structures, efficiency losses due to BO-CID could be higher than 2% absolute, ~11% relative [16], although typically in the range of 4–6% relative [14]. As the commercial PV industry is rapidly adopting PERC solar cell structures (they are expected to be mainstream from 2020 [1]), BO-CID could have a significant impact on global electricity generation from PV devices.

By 2025, predictions anticipate a global installed capacity for PV of more than 1 TW, with approximately 1500 TWh of PV-based electricity generation [17]. P-type Cz wafers are expected to maintain a similar proportion of PV production or

even increase market share [1]. Assuming a 40% usage of silicon substrates subject to the formation of BO defects, with a 5% relative performance loss, this could equate to an additional 30 TWh of electricity being required from other electricity sources. If such electricity is generated using fossil fuels, this could equate to unnecessary greenhouse gas emissions of $\sim 26\,640\,000$ tons CO_2 equivalent (CO_{2e}) (based on an average of 888 tons CO_{2e} per GWh of electricity production from coal [18]).

A number of potential avenues to avoid the formation of BO-related carrier-induced defects have been identified and described elsewhere, such as thermal processing, the use of other silicon materials with alternative dopants or lower oxygen concentrations. However, each of these can come with disadvantages, like added cost or introduction of different performance limiting defects or issues [4], [12], [19]–[36]. For example, the extent of BO-CID can be modulated by thermal processing such as by thermal diffusions or fast firing with rapid cooling. However, such processes have not yet demonstrated the complete elimination of CID [4], [5], [12], [37]–[39]. Without carrier injection, the recombination activity of the defect can be eliminated by annealing at elevated temperatures [2], [5], [31], [40]–[42]; however, subsequent illumination can re-form the defects, and hence the thermal annealing only results in a metastable recovery of the cell performance, as will be discussed in the next section on the BO defect system.

In 2006, Herguth *et al.* presented a breakthrough for the PV industry with a method for permanently eliminating BO-CID on conventional Cz wafers containing boron and oxygen [43]. This was based on an illuminated annealing process. However, the permanent recovery can also be achieved in the dark with current injection; hence, this permanent recovery is also a carrier-induced mechanism [44]. In recent years, a number of breakthroughs have led to the development of illuminated anneals using a laser for permanent recovery and stable cells in only 8 s.

First one is the identification of the role of hydrogen in the permanent deactivation process [45]–[50]. Subsequently, a mechanism for hydrogen passivation was provided by recognizing the importance of hydrogen charge states [29], [51]. High-speed regeneration processes were also presented on pre-degraded samples through increasing the illumination intensity to 2–3 suns [52]. Subsequently, defect formation was identified as a limiting factor for enabling high-speed processes on finished cells without the requirement to degrade samples prior [53]. These contributions have led to the development of multiple widely used commercial tools [54], [55], enabling manufacture of stable commercial cells and modules using boron doped Cz substrates.

Once passivated, the hydrogen–boron–oxygen (H-BO) complex is recombination inactive. This complex is stable under subsequent illumination, but it can be depassivated at elevated temperatures, therefore destabilizing the material [43], [52]. Due to the potential destabilization of the H-BO, questions over the stability of the passivation for applications in the field have been raised. Depending on conditions of installation, such destabilization could have negative impact on the warranties issued by solar panel manufacturers, which require that a certain

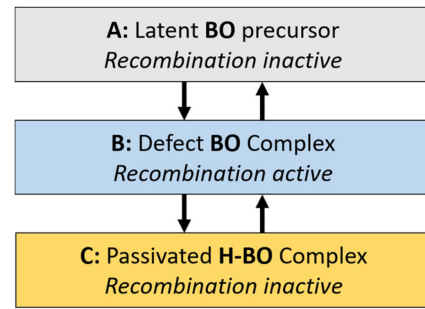


Fig. 1. Diagrammatic representation for the three-state hydrogen-based model for boron–oxygen defect complex system, associated with carrier-induced degradation in boron-doped Cz silicon.

level of performance be maintained for typically 25 years, with an expectation for even longer performance warranty periods from 2020 [1].

Expanding on earlier work in references [56], [57], here we investigate the performance loss for a worst case scenario numerical simulation of PV modules in the field, with a BO-CID mitigation process performed during manufacturing. We expand on previous work through highlighting the approximate ranges of reaction rates for module operating temperatures in the field, providing further analysis of weather data in the locations studied and a thorough investigation of the impact of module mounting systems on the BO defect system and hence concern for different solar panel applications. The study is based on experimentally obtained values for the destabilization reaction as published in the literature, and predicted module temperatures using the System Advisor Model (SAM) (version 2015.06.30) [58]–[60] fed with typical meteorological year version 2 (TMY2) data from Meteonorm V 5.0.13 [61] from four locations around the world.

To solve warranty concerns in regions where the passivation is likely to be less stable, it is possible to use these unfavorable conditions for passivation stability, reversing the process to capitalize on these conditions that also enable carrier-induced passivation. This work considers a self-repairing module concept [62] and investigates the potential in the field when no (or partial) BO-CID mitigation process is performed prior to installation. This is based on the same modeling principle, now including the other defect reactions in three-state BO defect system (to be discussed in the next section) as a best case scenario.

II. MODELING METHOD AND RESULTS

A. The BO Defect System

A three-state hydrogen-based model is used here to describe the BO defect complex system that is associated with CID in boron-doped Cz silicon, as has been used by various authors [44], [63]–[65]. The three-state model is likely to be an over-simplification of the full process [66], but is capable of adequately describing the process for practical purposes. A diagrammatic representation of the three-state system modeled in this work is shown in Fig. 1.

The first state (A) is comprised of a latent, recombination-inactive BO defect complex [67]. This state can be populated by annealing in the absence of charge carriers. The final process for the fabrication of silicon solar cells is the high-temperature fast-firing process for metallization. This is typically performed with little or no illumination, meaning that at the end of the process, the system is generally in state A. It should be noted, that stray light as the wafers leave the furnace can start to form defects, which can result in a small population in state B. The second state (B) describes the material in the degraded state, after the formation of the carrier-induced recombination-active BO defect complex from individual constituents of boron and oxygen. This typically occurs after exposure to carrier injection at relatively low temperatures. The third state (C) describes the silicon material once the recombination-active BO defects have been passivated by hydrogen, to form a recombination-inactive H-BO complex.

State C is typically achieved during an illuminated annealing process performed at elevated temperatures in the range of 100–300 °C [63], [68], [69]. A pre-requisite to achieving this state is the introduction of hydrogen into the bulk of the silicon [50], typically achieved during fast firing; although it should be noted that recent work has shown regeneration without deliberate introduction of hydrogen into the bulk [70]. However, in that work, the samples were still processed with hydrogen-containing solutions or hydrogen-containing dielectric layers. The authors noted that samples with an intentional introduction of hydrogen displayed the largest regeneration rates. State C is stable with exposure to subsequent minority carrier injection. It should be noted that at any given time, a mix of the states may be present in the silicon.

For the three-state model, only four transitions are assumed to be physically relevant. The transition from state A to B (Γ_{AB}), describes the formation of the recombination-active BO complex under carrier injection. The reverse transition from state B to A (Γ_{BA}) describes the thermal annealing of the recombination-active BO complex. The transition from state B to C (Γ_{BC}) describes the hydrogen passivation of the recombination-active BO complex to form a recombination-inactive H-BO complex. The transition from state C to B (Γ_{CB}) describes the thermal dissociation (destabilization) of the H-BO complex, back to a recombination-active BO defect complex that is isolated from hydrogen. Direct transitions between states C and A are assumed to be irrelevant for this system. It should be noted that in other studies, destabilization has been assumed to occur from state C directly to state A [44], [52]. The exact transition is not important for the key findings of this article. Further discussions addressing why we use a transition of state C to B can be found in [65]. A more detailed description of the overall system first described in [43] can be seen in [65].

For each transition Γ_{ij} , there exists an activation energy ($E_{a,ij}$) from state i to j to describe the temperature dependence of the reaction. There is also an associated attempt frequency (v_{ij}) for the reactions. The activation energies and attempt frequencies are shown in Table I for illumination intensities close to 1 sun, for solar cells with a bulk boron doping density

TABLE I
ACTIVATION ENERGIES (E_a) AND ATTEMPT FREQUENCIES (v_{ij}) FOR TRANSITIONS FROM STATE I TO J (Γ_{ij}) IN THE BORON-OXYGEN DEFECT COMPLEX SYSTEM, ASSOCIATED WITH CARRIER-INDUCED DEGRADATION IN BORON-DOPED CZOCHRALSKI SILICON

Process	Γ_{ij}	E_a (eV)	v_{ij} (s^{-1})	Ref.
Defect Formation	Γ_{AB}	0.475	4×10^3	[77]
Defect Dissociation	Γ_{BA}	1.32	1×10^{13}	[77]
Defect Passivation	Γ_{BC}	0.98	4.6×10^9	[52]
Destabilisation	Γ_{CB}	1.25	5×10^9	[52]

Values for the transitions Γ_{AB} and Γ_{BC} are shown under open circuit conditions in the vicinity of 1 sun.

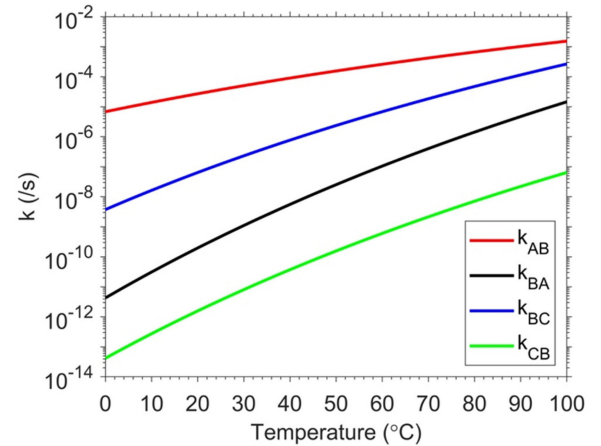


Fig. 2. Reaction rates for the boron–oxygen defect system between 0 and 100 °C using the attempt frequencies and activation energies as shown in Table I.

of $1 \times 10^{16}/\text{cm}^3$. The defect formation rate is expected to be independent of illumination intensities above 0.01 suns (assuming open circuit conditions), until approaching high injection, when a further acceleration of defect formation can be realized. It should be noted that the value of $v_{BC} = 4.6 \times 10^9 \text{ s}^{-1}$ is estimated at an illumination intensity of 1 sun in open circuit conditions on a standard screen-printed solar cell, with a full area Al-BSF. This is in agreement with a linear prorata estimate of the reaction rate using an illumination intensity of 2.7 suns in open circuit conditions shown in [52]. The activation energy for the transition Γ_{BC} is taken from the same reference.

The strong temperature dependence of the reactions in the BO defect system is shown in Fig. 2. For defect passivation (Γ_{BC}) and defect destabilization (Γ_{CB}), which are the two reactions of most interest in this article, even a small increase in temperature can significantly increase the reaction rates (k_{BC} and k_{CB} , respectively). For example, at 60 °C, an increase of 10 °C would increase the passivation reaction rate by a factor of 2.7 and the destabilization reaction rate by a factor of 3.6. This increase would reduce the time constant for those reactions by the same respective factors.

In this article, we assume a defect formation rate (k_{AB}) that is activated by illumination, but independent of the illumination intensity. This is valid for low-lifetime structures in

p-type silicon at illumination intensities in the vicinity of 1 sun and below, in which the defect formation rate saturates at low illumination intensities (approximately 0.1 suns) [4], [71]–[73]. This saturation occurs in p-type samples due to a sufficient availability of electrons for the defect formation reaction, while any subsequent increase in illumination intensity in this range will not substantially increase the total hole concentration. For such samples, substantially higher illumination intensities are required before the total hole concentration can be substantially increased, leading to an acceleration of defect formation [53].

It is also assumed that the passivation rate k_{BC} (where relevant) is in open circuit conditions and linearly dependent on the illumination intensity. Such open circuit conditions commonly occur when modules are installed but not yet connected or in operation. The linear dependence on the illumination intensity was chosen given that in [74] the reaction rate is approximately linear in the vicinity of 1 sun. The assumption of open circuit conditions is likely to provide a best case scenario for the time required for a natural passivation of BO defects that could occur under carrier injection in the field. In reality, the extraction of carriers under field operation will reduce the carrier concentrations, by one to two orders of magnitude, from that observed in open circuit conditions. This will most likely result in a reduction in v_{BC} by a similar magnitude. Thus, the timescales presented in this article only convey a qualitative comparison of the performance of modules between different mounting structures in different locations around the world. In reality, there are many factors that will influence the timescales for the reactions, including the injection level achieved in the cell [75] (dependent on cell performance), the thermal history of the cell (most notably the fast-firing profile used for contact firing [76], or any post-firing thermal processes [52]). Importantly, due to the substantially lower reaction rate for destabilization (k_{CB}) than thermal annealing (k_{BA}), this still results in effective passivation being obtainable despite a potentially small difference in the reaction rates of passivation and thermal annealing.

The annealing of the BO defect (Γ_{BA}) and defect destabilization (Γ_{CB}) reactions are assumed to only be dependent on temperature, based on experimental data from the literature [52], [77]. That is, the reactions occur with the same rate in darkness as well as under illumination. On the other hand, reactions Γ_{AB} and Γ_{BC} only occur with illumination or carrier injection. Hence, in reality, at module operating temperatures we only see the effects of Γ_{BA} and Γ_{CB} without illumination. For degradation (Γ_{AB}), due to the saturation of the degradation rate at very low illumination intensities as already mentioned, we assume a constant reaction rate under operating conditions. For defect passivation (Γ_{BC}), a linear dependence on the illumination intensity is used [74].

The normalized concentrations in each of the states ($N_i(t)$), where $i = A, B, C$, are governed by a system of linear differential equations given by (1)–(3) below [44], [64]. Here, k_{ij} is the rate constant from state i to j according to the Arrhenius equation, as shown in (4).

$$\frac{\delta N_A}{\delta t} = \kappa_{BA} \cdot n_B - \kappa_{AB} \cdot n_A \quad (1)$$

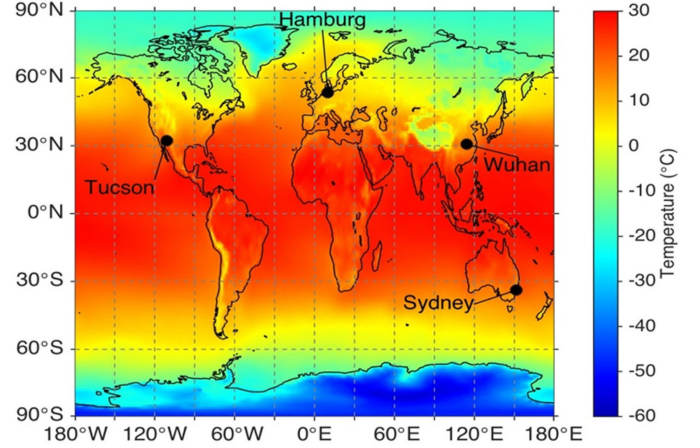


Fig. 3. Average annual surface air temperature (January 1951 and December 1980) across the globe using data from the Berkeley Earth Surface Temperature Project on a 1×1 grid [78]–[80].

$$\frac{\delta N_B}{\delta t} = \kappa_{AB} \cdot n_A + \kappa_{CB} \cdot n_C - (\kappa_{BA} + \kappa_{BC}) n_B \quad (2)$$

$$\frac{\delta N_C}{\delta t} = \kappa_{BC} \cdot n_B - \kappa_{CB} \cdot n_C \quad (3)$$

$$\kappa_{ij} = v_{ij} \cdot e^{-\frac{E_a}{k_b T}}. \quad (4)$$

B. Analysis of Meteorological Data

As the reactions in the BO defect system are temperature-dependent, it is important to understand the operating temperatures of modules in the field, in order to assess the long-term stability of CID mitigation in modules. Determining the actual operating temperature of modules in the field requires complex modeling, such as the SAM (version 2015.06.30) [58]–[60] used in this work, and is dependent on a large number of variables. Two key parameters that influence the operating temperature are the ambient temperature and solar insolation. Both of these differ substantially across the globe and throughout the year.

For the simulations performed in this work, four different locations with different yearly temperature and insolation conditions are used, as listed below:

- 1) Hamburg, Germany (53.5653°N, 10.0014°E).
- 2) Sydney, New South Wales, Australia (33.8650°S, 151.2094°E).
- 3) Tucson, Arizona, The United States of America (32.2217°N, 110.9264°W).
- 4) Wuhan, Hubei province, China (30.5833°N, 114.2833°E).

These four locations are subject to very different temperature distributions and solar insolation throughout the year. Fig. 3 shows the global distributions of the average annual surface air temperature between January 1951 and December 1980, as extracted from the *Berkeley Earth Surface Temperature Project* on a 1×1 grid [78]–[80]. Since 1980, global temperatures are increasing at 0.16 °C per decade [81], and not linearly across the globe [82], which overtime will somewhat change the global temperature distributions. However, the focus of this work is to show that different locations and mounting schemes,

TABLE II
AVERAGE SURFACE AIR TEMPERATURE FOR HAMBURG, SYDNEY, TUCSON,
AND WUHAN FROM METEONORM DATA USED IN THIS WORK, COMPARED
WITH THE LONG-TERM AVERAGE FROM JANUARY 1951 AND DECEMBER 1980
FROM THE BERKELEY EARTH SURFACE TEMPERATURE PROJECT

	Hamburg	Sydney	Tucson	Wuhan
Average long-term surface air temperature (°C)	8.6	17.8	17.9	16.8
Average ambient temperature (°C)	9.0	17.9	20.1	17.0
Difference (°C)	0.4	0.1	2.2	0.2

which therefore affect the module temperatures, will modulate how the panels respond to light-induced degradation. The image highlights that the long-term average temperature in the vicinity of Hamburg is substantially lower than that for the other three locations. As a result, it would be expected that Hamburg would suffer less from a potential destabilization of passivated BO defects than the other locations. However, the lower temperatures could also increase the time to passivate BO defects in the field.

C. Actual Weather Data Used

TMY2 from Meteonorm V 5.0.13 [61] was used for each of the locations, in hourly intervals for an entire year. TMY2 is a standard format of hourly meteorological data, used commonly in software packages to model the performance of PV systems. A TMY2 file for one year is a collection of “typical” months selected from a long-term data set, based on how close each month is compared to the statistics of the average observations for a particular month of the year. Meteonorm uses a combination of local weather observations in combination with models and long-term averages to create their TMY2 files, using data from the Global Energy Balance Archive, the World Meteorological Organization (WMO/OMM) Climatological Normals 1961–1990, and from MeteoSwiss [61].

An example data set of the ambient temperatures for Tucson is shown in Fig. 4(a) at hourly intervals throughout the year. The graph clearly shows the daily and seasonal variations in temperature. Fig. 4(b) shows the distributions of the ambient temperature in terms of the number of hours in each temperature range throughout the year, in 1 °C intervals. Sydney has a narrow temperature distribution with a peak at approximately 20 °C, while Tucson has the hottest temperature distribution and Hamburg has the coldest.

A summary of the average ambient temperature throughout the year for each of the locations is shown in Table II. The long-term average surface air temperature is also shown for each of the locations, as extracted from the data shown in Fig. 3. A general agreement is observed between the two values for each location (less than 2.2 °C), suggesting that the weather data used in this article for the simulations adequately represent the expected temperature distributions and the variations throughout a given year in each location to enable an interesting comparison between locations of varying climate. It should be noted that the exact weather data used in this article will lead to different

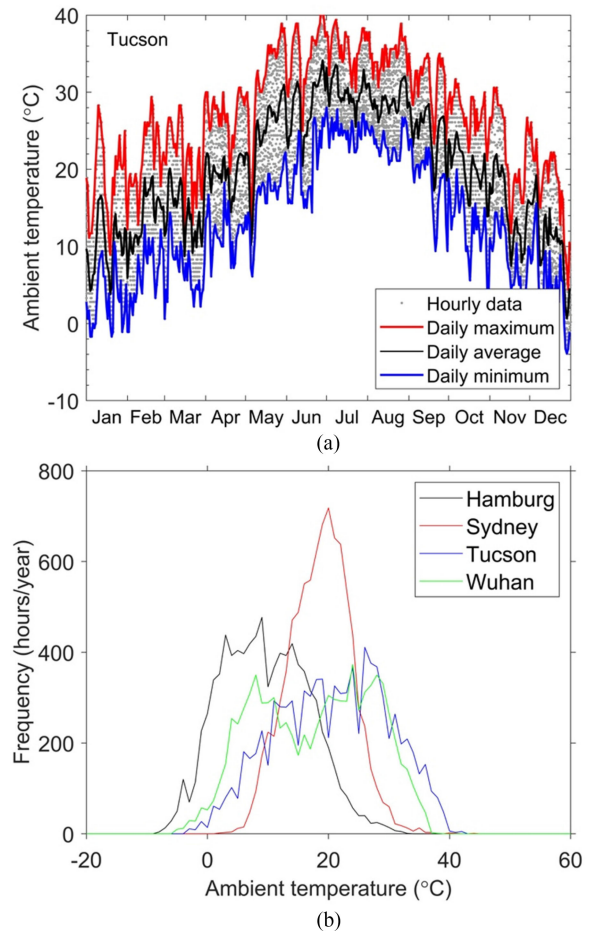


Fig. 4. (a) Hourly distribution of ambient temperatures in Tucson throughout the year. (b) Distribution of ambient temperatures throughout in hours per year in each 1 °C interval. Note that although the data are not continuous, it is presented as a line graph rather than a histogram for clarity of presenting all series on the same graph.

timescales for the reactions, but do not change the conclusions drawn in this article.

The yearly solar insolation greatly varies between the four locations investigated in this article. Table III shows a summary of the key solar insolation data for each location on two tilted angles. A tilt angle of 15° toward the equator was chosen for roof mounted PV arrays, while a tilt angle equivalent to the latitude facing the equator was used for large centralized PV installations. The average plane of array irradiance (POAI) for the module is the average insolation when exposed to sunlight over a year. The number of peak sunshine hours per day is the equivalent number of hours per day that the module is exposed to the nominal irradiance of $I_0 = 1000 \text{ W/m}^2$. Using this average solar irradiance value, the average attempt frequency v_{BC} for the passivation reaction was calculated assuming a linear dependence on the instantaneous illumination intensity (I) as shown in (5), where v_{BC,I_0} is the v_{BC} under nominal irradiance.

$$v_{BC}(I) = v_{BC,I_0} \left(\frac{I}{I_0} \right). \quad (5)$$

TABLE III
SOLAR INSOLATION DATA FOR HAMBURG, SYDNEY, TUCSON, AND WUHAN

	Sunshine hours/yr	Tilt of Array	Avg Solar Irradiation (POA hrs operation) (W/m^2)	Peak sunshine hours (/day)	Avg v_{BC} ($\times 10^9 \text{ s}^{-1}$)
Hamburg	4615	15°S 53.6°S	226.7 226.3	2.87 2.86	1.05 1.05
Sydney	4591	15°N 33.9°N	391.6 400.4	4.93 5.04	1.81 1.85
Tucson	4747	15°S 32.2°S	489.7 506.8	6.37 6.59	2.27 2.35
Wuhan	4685	15°S 30.6°S	330.1 328.5	4.24 4.22	1.52 1.52

TABLE IV
DESCRIPTION OF THE PHOTOVOLTAIC SYSTEM MODELED IN THIS ARTICLE

PV panels	12× 270 W mono panel, 16.68% at STC
Inverters	Enphase 250M Microinverters
Total capacity	3240 Wp
Configuration	2 rows of 6 panels
Tilt	15° or Latitude

As shown in Table III, Tucson is the sunniest location, and therefore has the highest average v_{BC} . Slight variations in the solar insolation and subsequent average v_{BC} are also noted between systems at the same location, depending on the tilt of the array. For Hamburg and Wuhan, almost no difference is observed between the different system tilts. However, for Sydney and Tucson, the solar insolation is increased when tilting the array at the latitude angle.

D. Influence of Installation on the Operating Temperature of PV Modules

In this section, the operating temperature of modules in the field is simulated based on the meteorological data for ambient temperature and solar irradiance incident on the plane of array (POA) of the module on an hourly basis for an entire year.

The system used for the modeling consisted of 12 × 270 W monocrystalline silicon PV panels with an efficiency of 16.68% under standard test conditions (STCs) of 25 °C, 1000 W/m^2 , as nominated by the module manufacturer. A summary of the key system parameters is shown in Table IV. It is assumed that the nominal efficiency is that after the full formation of BO defects, and therefore of the module in the degraded state.

Three different mounting schemes for the system are investigated in this work. First, a building-integrated photovoltaic system (BIPV) that is mounted flush with the roof, tilted at 15°. This system has no ventilation at the back of the modules to assist with cooling and should experience the highest operating temperatures. Second, a rack-mounted system on a roof tilted at 15° (PV-R), with a 100-mm air gap at the back of the modules to allow some ventilation for cooling. Third, a rack-mounted system installed on a flat ground for a large centralized PV system, tilted at the latitude toward the equator (PV-C). This system has full ventilation at the rear of the module to assist with cooling, and hence should experience the lowest operating temperatures.

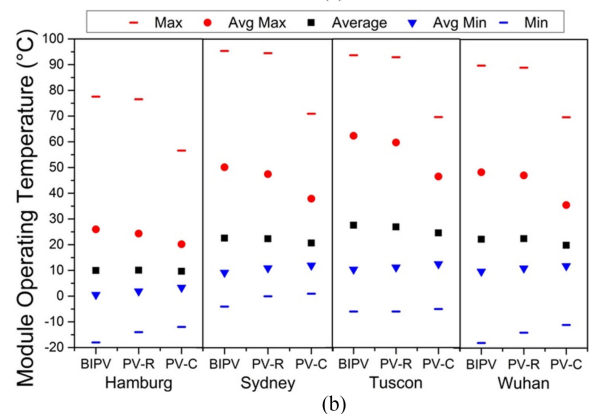
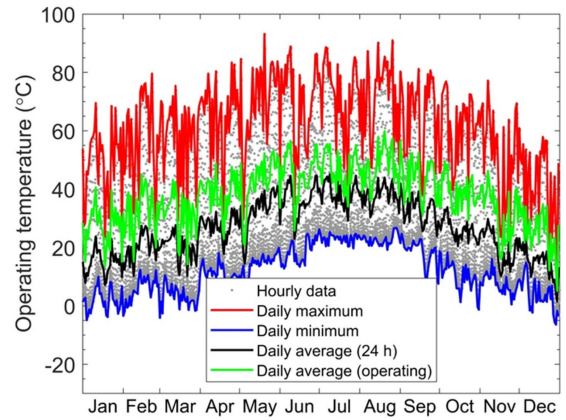


Fig. 5. (a) Hourly module temperature on a rack-mounted system installed in Tucson on a roof tilted at 15° with a 100-mm air gap (PV-R). (b) Module temperature data for each location (Hamburg, Sydney, Tucson, and Wuhan), and each type of mounting (BIPV, PV-R, and PV-C) showing yearly average, maximum, minimum, and daily average maximum and minimum.

Simulations for the output power, efficiency, and temperature of the modules in operation were obtained using the SAM (version 2015.06.30) from the National Renewable Energy Laboratory (NREL) [58]–[60].

1) *Module Operating Temperatures*: The SAM model output for PV systems installed at the four different locations, highlights the substantial daily and seasonal differences in the operating temperatures for each location and mounting types. Fig. 5(a) shows the modeled temperature data in hourly intervals (gray dots) for an entire year of operation of a rack-mounted roof system with a 100-mm air gap (PV-R) in Tucson. It also shows the minimum and maximum operating temperature for each day (blue and red lines, respectively), the daily average over 24 h (black line) and the daily average only including the hours of operation (green line). This image highlights the substantial increase in module temperature above the ambient temperature during operation [see Fig. 5(a) for the comparison]. Fig. 5(b) shows the average yearly module temperatures, as well as maximum, minimum, average daily maximum and minimum for BIPV, rack roof mount (PV-R), and centralized flat ground (PV-C) systems in each location. This highlights the substantial differences in the module temperatures for each location for the different mounting structures. A well-ventilated

TABLE V
MODELED OPERATING TEMPERATURE DATA FOR PHOTOVOLTAIC SYSTEMS
INSTALLED IN HAMBURG, SYDNEY, TUCSON, AND SYDNEY

		T_{\max} (°C)	Av. Daily T_{\max} (°C)	Av. Op. T (°C)	Av. Temp (incl. night-time)	Hrs over 50°C
Hamburg	BIPV	79.3	27	14.9	10	165
	PV-C	57.4	20.9	12.9	9.7	17
	PV-R	78.5	25.4	14.3	10.1	140
Sydney	BIPV	96.8	51.1	32.6	22.6	826
	PV-C	71.9	38.6	26.9	20.7	162
	PV-R	95.9	48.6	31	22.4	645
Tucson	BIPV	94	63.6	39.6	27.5	1619
	PV-C	70.7	47.4	32.4	24.6	554
	PV-R	93.2	61.1	37.8	26.9	1332
Wuhan	BIPV	89.9	49.7	31.4	22.3	975
	PV-C	69.8	36.4	25.5	20	256
	PV-R	89.1	48.4	31	22.5	889

ground mounted system (PV-C) experiences substantially lower operating temperatures (particularly maximums) throughout the year than a BIPV system, or a rack-mounted system on a tilted roof with only a 100-mm air gap (PV-R). In locations other than Hamburg, PV-R and BIPV systems reach temperatures approaching 100 °C, with average daily maximums as high as 60 °C. Note that we have not included temperatures during the night, as without illumination the modules are typically at ambient temperature, which is substantially lower than module operating temperature during the day, and hence destabilization reactions are insignificant.

A summary of the key temperature data for the four locations is shown in Table V. Sydney experiences the highest maximum temperature throughout the year for each mounting structure, reaching up to 96.8 °C for a BIPV system, while Tucson has the highest average of the daily maximum temperatures throughout the year and the highest number of operating hours over 50 °C for each mounting structure. By far, Hamburg has the lowest operating temperatures. A PV-C system installed in Hamburg only experiences 17 h with an operating temperature above 50 °C, while a similar system installed in Tucson will experience 554 h. As a result, it is expected that Hamburg will provide the most suitable environment for avoiding the destabilization of passivated BO defects; however, the worst for the self-repairing module which relies on temperature as well as carrier injection for the passivation of BO defects in the field. In contrast, Tucson is expected to suffer the most from a destabilization of passivated BO defects, while it has the best location for a self-repairing module due to the fastest passivation of BO defects in the field.

For laboratory studies investigating the BO defect system, setups are usually established to decouple the influence of illumination from the influences of temperature changes. For example, when varying the illumination intensity, the set point on a hotplate may need to be altered to maintain a constant wafer temperature [53]. However, in the field, the illumination intensity and operating temperature of the modules are closely coupled. Fig. 6 shows example distributions of the operating temperatures of modules as a function of solar insolation for a PV-R system in Sydney and a BIPV system in Wuhan. While

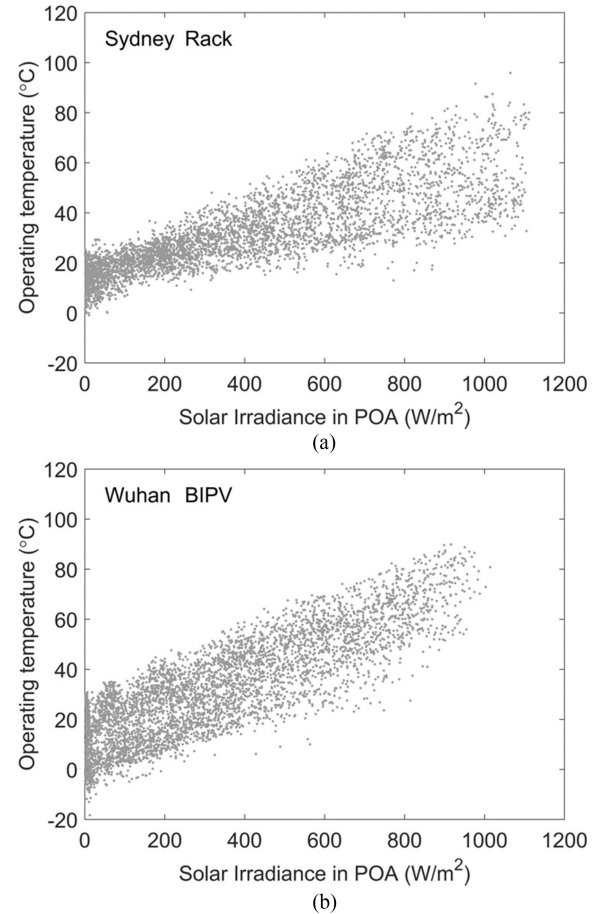


Fig. 6. Effect of solar irradiation in the plane of array (POA) on the operating module temperature for (a) a PV-R system in Sydney, and (b) a BIPV system in Wuhan.

there are many other factors that influence the actual operating temperature of the module, the solar insolation in the POA has a significant impact. The coefficients of temperature increase for all scenarios were in the range of approximately (30–60) mK/W/m². The lowest temperature coefficient of 30 mK/W/m² in Sydney for a PV-C system would result in an increase of the exponential component of the reaction rate by a factor of 24 when increasing the illumination intensity from 100 to 1000 W/m². For the highest temperature coefficient of 62 mK/W/m², the corresponding increase in the exponential component of the reaction is a factor of 570. In contrast, the attempt frequency would increase in both cases by a factor of 10. This suggests that the induced temperature increase from illumination will have a significantly larger impact in accelerating the reaction rate (particularly for defect passivation), than the dependence directly on carrier injection through increases in the attempt frequency.

E. Modeling the Destabilization of Passivated BO Defects

In this section, we perform simulations over a 40-year period for the various locations and mounting structures on modules that have had the BO defects fully passivated during the manufacturing process. A MATLAB ordinary differential equation

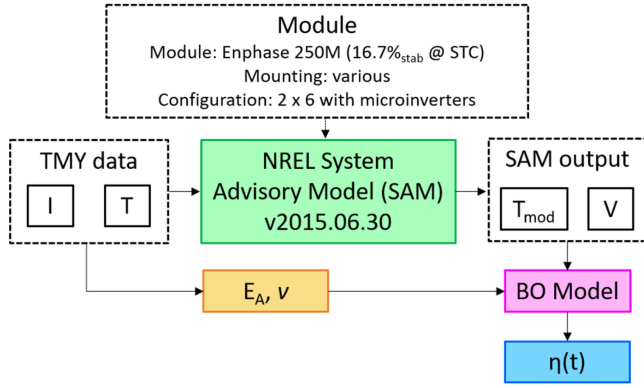


Fig. 7. Diagrammatic representation of the model used in this article.

(ODE) solver (ode15 s) was used with a maximum time step of 1 h, using the system of equations presented in (1)–(4), for the BO defect system and the relevant reaction rates from Table I. Input temperatures were based on the hourly data fed from the output of the SAM model. For calculations at intermediate times, a linear interpolation of the modeled temperature was used. Fig. 7 shows a diagrammatic representation of the model used in this article to predict module efficiency. The predicted module operating temperature and reaction rates were fed into the BO defect model, taking into account a potential dependence of the defect passivation rate on the illumination intensity (I). The output of the BO model was then used to predict the efficiency (η) as a function of time.

It was assumed at the start of each simulation that 100% of the defects were passivated, and hence ($N_C(t = 0) = 1$). For the simulation, as a worst case scenario, the passivation reaction was disabled. Under this regime, any passivated defects (H-BO complexes) that are thermally destabilized due to operation in the field at elevated temperatures, are not re-passivated. Therefore, any destabilization of defects results in the degradation of the cell performance. This would be the case if, when a module is put in the field, no further atomic hydrogen is available within the silicon for BO defect passivation. A number of factors could act to reduce the concentration of hydrogen available for BO defect passivation such as:

- 1) The effusion of hydrogen out of the silicon solar cell;
- 2) An evolution of atomic hydrogen into a state that is not available for passivation (such as the formation of molecular hydrogen);
- 3) Passivation of other defect species.

The passivated defects that were destabilized were assumed to all move into the recombination active state (state B), and hence cause a degradation of the module performance. This is justified, as any elevated operating temperature will occur in the presence of carrier injection, and therefore enable defect formation. Furthermore, for any temperature below 100 °C, under steady-state conditions, using the reaction rates in Table I, less than 1% of defects would shift back to a recombination inactive state (state A).

A performance loss to CID of 5% relative was assumed for the modules, with a module efficiency of 16.68% at STC conditions

in the fully degraded state. This level of 5% relative degradation is typical for the expected power loss due to BO defects [83], [29], [56]. Therefore, the absolute potential efficiency loss due to CID was assumed to be 0.88%, with a corresponding efficiency of a module with 100% of BO defects in the passivated state being 17.56%.

The fraction of recombination active defects in state B was then converted to an absolute efficiency loss due to light induced degradation (LID). This assumed that the efficiency loss was directly proportional to the drop in implied open circuit voltage of lifetime test structures throughout the defect formation process and was calculated according to (6).

$$\text{relative efficiency loss} = \frac{V_{OC}(t = 0) - V_{OC}(t)}{V_{OC}(t = 0)}. \quad (6)$$

The output of the model suggests that both the mounting structure and location could have a significant impact on the potential stability of the passivation (see Fig. 8). BIPV-integrated systems show the largest potential destabilization of the passivated BO defects, which could cause up to a 0.4% absolute efficiency loss after 40 years for a BIPV system in Tucson. In contrast, a 0.05%, 0.15%, and 0.25% absolute efficiency loss could occur in Hamburg, Sydney, and Wuhan, respectively. PV-R systems are expected to have slightly lower efficiency losses than BIPV systems. In contrast, the PV-C systems show no significant sign of potential degradation, with less than 0.05% absolute efficiency loss after 40 years in all locations. A close look at the plots shows stepped degradation due to seasonal variations, with the majority of degradation occurring during the summer months, and the efficiency of the modules being relatively stable during the winter months. The corresponding overall energy yield loss over 40 years in Sydney is depicted in Fig. 8(d) as an example case study. When compare to a nominal yield of 7.74×10^7 kWh over 40 years as assumed from the passivated case, a relative loss in energy yield of 0.488%, 0.4%, and 0.058% is predicted given BIPV, PV-R, and PV-C systems, respectively.

The 0.4% absolute efficiency loss for modules BIPV modules in Tucson over 40 years is significant, and likely to be 0.8% absolute, or higher, for higher efficiency PERC structures which can suffer more than twice as much from destabilization [16]. This efficiency loss corresponds to a destabilization of 36% of passivated BO defects (H-BO). These results are based on the destabilization activation energy $\Gamma_{CB} = 1.25$ eV reported in [52], which has an uncertainty of ± 0.05 eV. At the extremes of this uncertainty, the destabilization reaction rate k_{CB} , could be as low as 1.20 eV or as high as 1.30 eV, which could result in a shift in the reaction rates according to Fig. 9. Over 40 years in the field, this could lead to significantly more or less destabilization respectively. For example, at the extremes of the uncertainty, a module at 50 °C for 40 years (which would overestimate the destabilization) the BO system destabilization could be as much as 0.04% with $E_a = 1.20$ eV, or as little as 0.01% for $E_a = 1.30$ eV. However, the trends between locations and mounting types would remain.

The estimated destabilization rates (k_{CB}) based on the mean temperature ($k_{CB,m}$), temperature data throughout the year

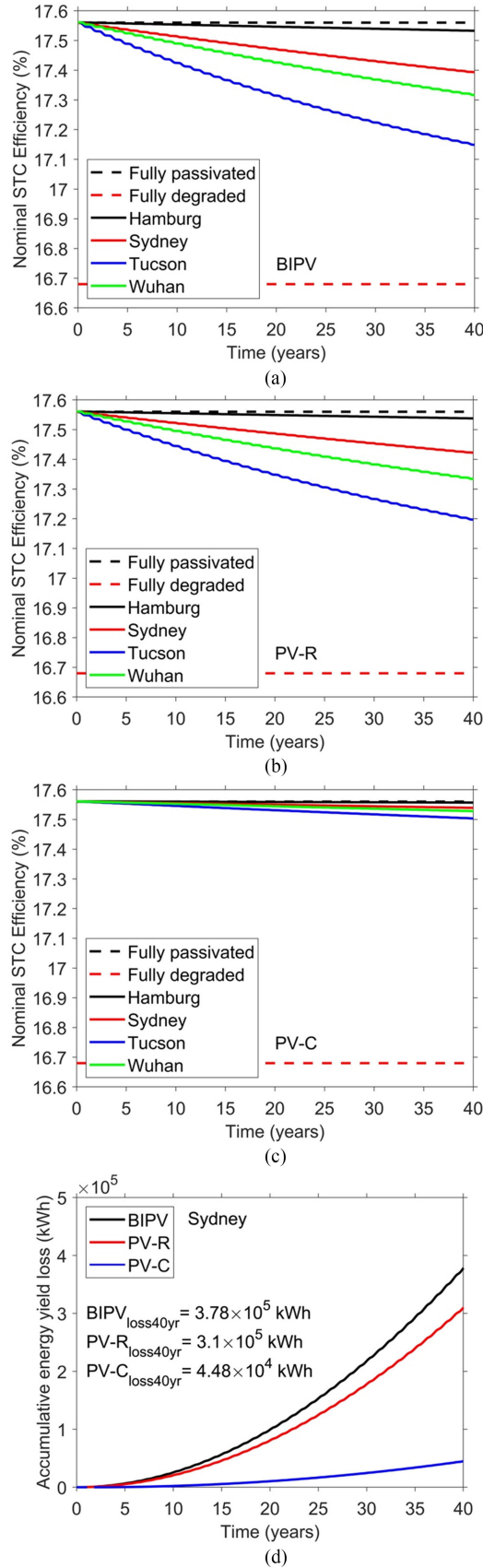


Fig. 8. Module efficiencies as a result of H-BO destabilization in each location for (a) BIPV, (b) Rack roof mounted (PV-R) installations, and (c) Centralized system on flat ground (PV-C). (d) The resulting loss in energy yield in Sydney as a function of time.

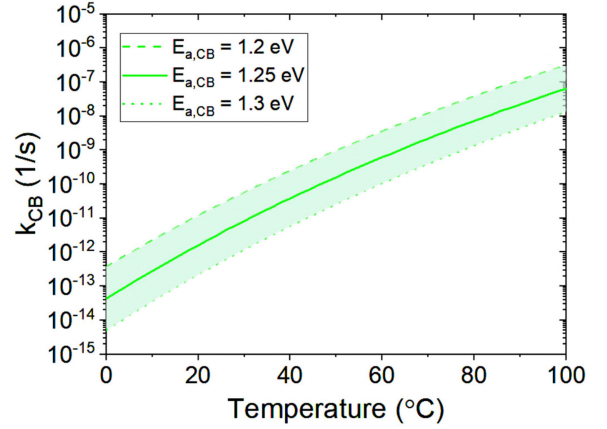


Fig. 9. Possible range of reaction rates for destabilization passivated boron-oxygen defects between 0°C and 100°C based on uncertainty in activation energy from [52].

TABLE VI
ESTIMATED DESTABILIZATION RATE (k_{CB}) FROM T_{mean} OF YEAR ($k_{CB,m}$), EXPECTED ($k_{CB,ex}$), AND ESTIMATED FROM MODEL ($k_{CB,es}$), AND ERROR

		$k_{CB,m}$ ($\times 10^{-12}$ /s)	$k_{CB,ex}$ ($\times 10^{-12}$ /s)	$k_{CB,es}$ ($\times 10^{-12}$ /s)	error (%)
	BIPV	27.2	16.9	16.8	0.6
Hamburg	PV-R	25.8	2.34	2.37	1.2
	PV-C	27.8	13.9	13.8	1.2
Sydney	BIPV	244	117	111	5.1
	PV-R	178	12.8	12.9	0.6
Tucson	PV-C	235	95.2	89.6	6.2
	BIPV	547	366	350	4.5
Wuhan	PV-R	337	34.7	34.9	0.7
	PV-C	494	308	292	5.2
Wuhan	BIPV	232	180	174	3.6
	PV-R	157	19.8	19.6	1.0
	PV-C	242	164	159	3.6

($k_{CB,ex}$), and based on model ($k_{CB,es}$) under different mounting systems and locations are shown in Table VI. The error of the destabilization rates were calculated based on the difference between $k_{CB,es}$ and $k_{CB,ex}$. Location Tucson, which showed the most destabilization over 40 years (see Fig. 8) had an error up to 5.2%.

Although the instantaneous destabilization rate varies by orders of magnitude throughout each day and throughout the year, an effective destabilization rate ($k_{CB,eff}$) for the worst case scenario of destabilization can be obtained. This $k_{CB,eff}$ value is defined as the equivalent destabilization reaction rate, k_{CB} , which results in the same level of destabilization after the 40-year period as modeled using the temporally varying temperature data (neglecting defect formation, defect dissociation, and any passivation reaction). This is valid over the

long-term (40 years), as the temperature variation, and therefore instantaneous reaction rate variation, is cyclic on a much shorter timescale (annually). Therefore, any seasonal influences have a small impact at the end of the 40 years. Furthermore, given that the operating temperatures are all below 100 °C, no significant defect dissociation occurs, so any destabilized defects will remain in a recombination active state.

An expected destabilization rate $k_{CB,ex}$ can be obtained from the yearly average of the instantaneous k_{CB} values calculated for each time temperature data using (7), where h is the hour and H represents the total number of hours in the year.

$$k_{CB,ex} = \frac{1}{H} \sum_{h=1}^H v_{CB} \cdot e^{\left(\frac{-E_{a,CB}}{k_B T_h}\right)}. \quad (7)$$

As shown, for all scenarios the $k_{CB,ex}$ value has less than a 7% deviation from the respective $k_{CB,eff}$ value. This suggests that the $k_{CB,ex}$ can provide a reasonably accurate estimation of the simulated destabilization. In contrast, estimating a k_{CB} value from the average temperature throughout the year can lead to an under-estimation of the extent of destabilization in the simulation. This is due to the strong non-linear temperature dependence of the destabilization, which is heavily weighted toward the highest temperatures.

For the BIPV module installed in Tucson with 36% BO destabilization, $k_{CB,ex}$ is $3.66 \times 10^{-10} \text{ s}^{-1}$. This might be tolerable for the modules in this work with 0.4% abs efficiency loss over 40 years. However, for future higher efficiency structures, where efficiency losses could more than double due to BO defects, it would be preferable to limit destabilization to less than 10% over 40 years. This corresponds to an absolute efficiency loss of 0.13% abs for the modules in this work. To achieve this, the expected annually averaged rate of $k_{CB,ex}$ should be below $8.3 \times 10^{-11} \text{ s}^{-1}$.

F. Long-Term Passivation of BO Defects in the Field—A Self-Repairing Module

Under the same conditions of increased temperature and illumination that cause higher rates of destabilization, there is also the potential for natural passivation of BO defects in the module, if a source of hydrogen exists for passivation. Based on the same data shown previously, the expected rates for passivation for given conditions can be determined. Unlike destabilization processes which happen over decades in field conditions, the rates of passivation are much faster, so the time frames are highly dependent on the time of year. Fig. 10 shows the hydrogen passivation of BO defects in the field of an initially fully degraded module (0% passivated defects, $0 N_C(t)$) for a roof mounted system in Sydney. From (a), it is clear that a module installed in winter takes much longer to achieve full passivation of BO defects, as the time to achieve full passivation ($1 N_C(t)$) is much longer between May and August, and an order of magnitude longer than a module installed in January (Summer in Sydney). Note that the fine horizontal-line structure is a result of changes in the BO defect system only occurring during the day with elevated module temperatures. that is, no substantial changes occur during the night. Fig. 10(b) shows

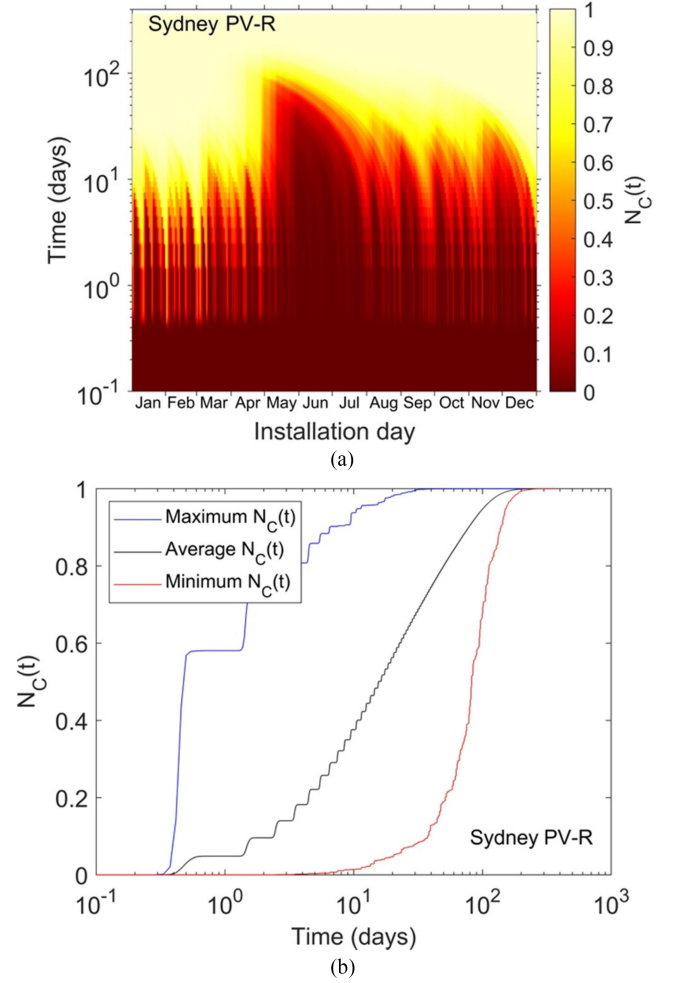


Fig. 10. (a) The field passivation of BO defects for a rack-mounted system Sydney following installation of a fully degraded module (0% passivated defects, $0 N_C(t)$). (b) The passivation trends for the minimum, maximum, and average times required for passivation depending on the time of year of install. That is, simulations were performed for installing modules on each day of the year.

the passivation trends for the minimum, maximum, and average times required for passivation to a certain fraction of defects (N_C) for simulations with modules installed on each day of the year. A fully degraded module can be almost completely passivated in two weeks in summer but takes months in winter. For the case that requires the minimum time for passivation, the process is very rapid where over 50% of defects can be passivated in one summer day (seen by the big jump), but then a clear level step while the module is in the dark overnight. On average, it will take 15.6 d to passivate half of the defects and in the worst case scenario when installed in May (late autumn), 82.5 d are required. Furthermore, given the known dependence of the passivation reaction on carrier concentration, this is particularly important for how long a module sits idle in the field before operation under open circuit conditions as has been assumed in this simulation. During operation at maximum power point, when the injection level is lowered significantly, the passivation rate is significantly lowered, which would increase the time required for regeneration.

Hydrogen can be introduced into a PV cell through typical screen-print firing processes of a cell with SiN_x passivation [84]. However, one should note that low-temperature approaches like HIT technology [85] or metallization by plating might be problematic due to a lower indiffusion of hydrogen. [86].

For installations likely to subject the modules to higher temperatures and illumination (with high $k_{CB,ex}$ values above a tolerable level $\sim 8.3 \times 10^{-11} \text{ s}^{-1}$) rather than provide fully passivated modules where the H-BO could destabilize with time, it could be preferable for manufacturers to offer “self-repairing” modules. Similarly, there may be installations where the field passivation is fast enough that the short-term power losses in the field may be more economically favorable than the cost of passivation during manufacturing. Such self-repairing modules would ensure hydrogen is available in a form suitable for passivation and optionally without complete passivation for the process to be completed in the field. As recent works have suggested, hydrogen is very likely to be a precursor for a different form of longer term degradation referred to as light and elevated temperature-induced degradation (LeTID) [87], either as a hydrogen containing complex or causing recombination on its own [88]–[94]. Thus, processes for incorporating hydrogen should be controlled and monitored, and testing conducted to determine the implications for potential LeTID. However, for modules installed in cooler climates, a large uncertainty in the time required to recover from LID may favor passivation of the defects during module production.

In any case, to avoid excessive destabilization in the field it would be preferable to ensure a suitable source of hydrogen remains in the silicon for subsequent passivation. In this way, whether or not the module is fully recovered prior to installation, any future destabilization that occurs can be self-repaired through the same conditions that cause the destabilization. As the passivation rates are faster than the destabilization rates in such field conditions, the module should always be able to self-repair, as long as sufficient hydrogen exists. For high-efficiency cell structures whose processes do not include high-temperature steps to incorporate hydrogen, this would require an optimized hydrogen incorporation step.

III. CONCLUSION

This article has modeled BO defect reactions including destabilization and passivation, using a three-state model based on experimentally obtained values as published in the literature. The SAM (version 2015.06.30) was fed with TMY2 data from four locations around the world to predict module operating temperatures for three types of mounting at each of four locations around the world. Mountings investigated were: a BIPV system that is mounted flush with the roof, tilted at 15° ; a rack-mounted system on a roof tilted at 15° (PV-R), with a 100-mm air gap at the back of the modules; and a rack-mounted system installed on a flat ground for a large centralized PV system, tilted at the latitude toward the equator (PV-C). Locations investigated were Hamburg, Sydney, Tucson, and Wuhan. Module operating temperatures are highly dependent on location and mounting. A BIPV module in Tucson reaches temperatures as high as 94°C , and has over 1600

h per year above 50°C . In this location, the high temperatures and illumination could cause modules installed in this way to have over one-third of their passivated BO defects destabilized. This destabilization results in a 0.4% absolute efficiency loss for the modules in this article, but it could be twice this amount with the shift to higher efficiency cells and modules. Passivation of BO defects can occur in the field if hydrogen is present. For modules that experience such extreme sustained conditions, cells/modules should be manufactured to ensure incorporation of hydrogen to enable passivation of BO defects in the field thereby enabling a “self-repairing module.” For a fully degraded module, the self-repairing processes can passivate the BO defects in as little as two weeks in the field but is extremely dependent on the mounting and location of the systems.

REFERENCES

- [1] ITRPV, “International technology roadmap for photovoltaic (ITRPV),” 2019.
- [2] H. Fischer and W. Pschunder, “Investigation of photon and thermal induced changes in silicon solar cells,” in *Proc. 10th IEEE Photovolt. Spec. Conf.*, 1973, p. 404.
- [3] J. H. Reiss, R. R. King, and K. W. Mitchell, “Characterization of diffusion length degradation in Czochralski silicon solar cells,” *Appl. Phys. Lett.*, vol. 68, no. 23, pp. 3302–3304, 1996.
- [4] J. Schmidt and K. Bothe, “Structure and transformation of the metastable boron- and oxygen-related defect center in crystalline silicon,” *Phys. Rev. B*, vol. 69, no. 2, p. 024107, 2004.
- [5] J. Knobloch *et al.*, “Solar cells with efficiencies above 21% processed from Czochralski grown silicon,” in *Proc. Conf. Record 25th IEEE Photovolt. Spec. Conf.*, 1996, pp. 405–408.
- [6] S. W. Glunz, E. Schaffer, S. Rein, K. Bothe, and J. Schmidt, “Analysis of the defect activation in Cz-silicon by temperature-dependent bias-induced degradation of solar cells,” in *Proc. 3rd World Conf. Photovolt. Energy Convers.*, vol. 1, 2003, pp. 919–922.
- [7] T. Niewelt, J. Schon, W. Warta, S. W. Glunz, and M. C. Schubert, “Degradation of crystalline silicon due to boron-oxygen defects,” *IEEE J. Photovolt.*, vol. 7, no. 1, pp. 383–398, Jan. 2017.
- [8] V. V. Voronkov, R. Falster, B. Lim, and J. Schmidt, “Permanent recovery of electron lifetime in pre-annealed silicon samples: A model based on Ostwald ripening,” *J. Appl. Phys.*, vol. 112, no. 11, p. 113717, 2012.
- [9] C. Möller and K. Lauer, “Light-induced degradation in indium-doped silicon,” *Phys. Status Solidi - Rapid Res. Lett.*, vol. 7, no. 7, pp. 461–464, 2013.
- [10] D. C. Walter *et al.*, “Effect of rapid thermal annealing on recombination centres in boron-doped Czochralski-grown silicon,” *Appl. Phys. Lett.*, vol. 104, no. 4, p. 042111, 2014.
- [11] L. I. Murin *et al.*, “The oxygen dimer in Si: Its relationship to the light-induced degradation of Si solar cells?” *Appl. Phys. Lett.*, vol. 98, no. 18, p. 182101, 2011.
- [12] S. W. Glunz, S. Rein, W. Warta, J. Knobloch, and W. Wetling, “Degradation of carrier lifetime in Cz silicon solar cells,” *Sol. Energy Mater. Sol. Cells*, vol. 65, no. 1, pp. 219–229, 2001.
- [13] D. Macdonald *et al.*, “Light-induced boron-oxygen defect generation in compensated p-type Czochralski silicon,” *J. Appl. Phys.*, vol. 105, p. 093704, 2009.
- [14] E. Cho *et al.*, “Light-induced degradation free and high efficiency p-type indium-doped PERC solar cells on Czochralski silicon,” in *Proc. IEEE 42nd Photovolt. Spec. Conf. (PVSC)*, 2015, pp. 1–4.
- [15] A. Herguth, R. Horbelt, S. Wilking, R. Job, and G. Hahn, “Comparison of BO regeneration dynamics in PERC and Al-BSF solar cells,” *Energy Proc.*, vol. 77, pp. 75–82, 2015.
- [16] D. C. Walter, B. Lim, and J. Schmidt, “Realistic efficiency potential of next-generation industrial Czochralski-grown silicon solar cells after deactivation of the boron-oxygen-related defect center,” *Prog. Photovolt. Res. Appl.*, vol. 24, no. 7, pp. 920–928, 2016.
- [17] IEA, “Snapshot of global PV markets 2014,” Int. Energy Agency, IEA-OECD, Rep. IEA PVPS T1-26:2015, 2014.
- [18] World Nuclear Association, “Comparison of lifecycle greenhouse gas emissions of various electricity generation sources,” Jul. 2011.

- [19] K. Ramspeck *et al.*, "Light induced degradation of rear passivated mc-Si solar cells," in *Proc. 27th Eur. Photovolt. Sol. Energy Conf.*, vol. 1, 2012, pp. 861–865.
- [20] J. R. Davis Jr. *et al.*, "Impurities in silicon solar cells," *IEEE Trans. Electron Devices*, vol. 27, no. 4, pp. 677–687, 1980.
- [21] K. Morita and T. Miki, "Thermodynamics of solar-grade-silicon refining," *Intermetallics*, vol. 11, pp. 1111–1117, 2003.
- [22] V. Meemongkolkiat *et al.*, "Resistivity and lifetime variation along commercially grown Ga- and B-doped Czochralski Si ingots and its effect on light-induced degradation and performance of solar cells," *Prog. Photovolt. Res. Appl.*, vol. 14, no. 2, pp. 125–134, 2006.
- [23] M. Forster *et al.*, "Ga co-doping in Cz-grown silicon ingots to overcome limitations of B and P compensated silicon feedstock for PV applications," *Phys. Status Solidi*, vol. 8, no. 3, pp. 678–681, 2011.
- [24] R. J. Falster, D. Gambaro, M. Cornara, M. Olmo, and M. Pagani, "Effect of high temperature pre-anneal on oxygen precipitates nucleation kinetics in Si," *Solid State Phenom.*, vol. 57, pp. 123–128, 1997.
- [25] P. E. Freeland, K. A. Jackson, C. W. Lowe, and J. R. Patel, "Precipitation of oxygen in silicon," *Appl. Phys. Lett.*, vol. 30, no. 1, pp. 31–33, 1977.
- [26] V. V. Voronkov and R. Falster, "Grown-in microdefects, residual vacancies and oxygen precipitation bands in Czochralski silicon," *J. Cryst. Growth*, vol. 204, pp. 462–474, 1999.
- [27] P. J. Cousins *et al.*, "Generation 3: Improved performance at lower cost," in *Proc. 35th IEEE Photovolt. Spec. Conf.*, 2010, pp. 275–278.
- [28] J. Haunschild, J. Broisch, I. Reis, and S. Rein, "Quality control of Czochralski grown silicon wafers in solar cell production using photoluminescence imaging," in *Proc. 26th Eur. Photovolt. Sol. Energy Conf. Exhib.*, 2011, pp. 1–6.
- [29] B. Hallam *et al.*, "Eliminating light-induced degradation in commercial p-type Czochralski silicon solar cells," *Appl. Sci.*, vol. 8, no. 1, p. 10, 2017.
- [30] W. Zulehner, "Czochralski growth of silicon," *J. Cryst. Growth*, vol. 65, no. 1, pp. 189–213, 1983.
- [31] J. Schmidt, A. G. Aberle, and R. Hezel, "Investigation of carrier lifetime instabilities in Cz-grown silicon," in *Proc. 26th IEEE Photovolt. Spec. Conf.*, 1997, pp. 13–18.
- [32] J. Schmidt, "Light-induced degradation in crystalline silicon solar cells," *Solid State Phenom.*, vol. 95, pp. 187–196, 2003.
- [33] D. W. Cunningham, A. Parr, J. Posbic, and B. Poulin, "Performance comparison between BP solar mono²™ and traditional multicrystalline modules," in *Proc. 23rd Eur. Photovolt. Sol. Energy Conf.*, 2008, pp. 2829–2833.
- [34] B. L. Sopori, "Defect clusters in silicon: Impact on the performance of large-area devices," *Mater. Sci. Forum*, vol. 258–263, pp. 527–534, 1997.
- [35] W. Schröter *et al.*, "Atomic structure and electronic states of nickel and copper silicides in silicon," *Mater. Sci. Eng. B*, vol. 72, no. 2, pp. 80–86, 2000.
- [36] O. Schultz, S. W. Glunz, S. Riepe, and G. P. Willeke, "High-efficiency solar cells on phosphorus gettered multicrystalline silicon substrates," *Prog. Photovolt. Res. Appl.*, vol. 14, pp. 711–719, 2006.
- [37] S. W. Glunz, S. Rein, J. Y. Lee, and W. Warta, "Minority carrier lifetime degradation in boron-doped Czochralski silicon," *J. Appl. Phys.*, vol. 90, p. 2397, 2001.
- [38] H. Nagel, A. Merkle, A. Metz, and R. Hezel, "Permanent reduction of excess-carrier-induced recombination centers in solar grade Czochralski silicon by a short yet effective anneal," in *Proc. 16th Eur. Photovolt. Sol. Energy Conf.*, 2000, pp. 1197–1200.
- [39] T. Saitoh *et al.*, "Suppression of light degradation of carrier lifetimes in low-resistivity CZ-Si solar cells," *Sol. Energy Mater. Sol. Cells*, vol. 65, no. 1, pp. 277–285, 2001.
- [40] K. Graff and H. Pieper, "The properties of iron in silicon," *J. Electrochem. Soc.*, vol. 128, p. 669, 1981.
- [41] B. Lim, S. Hermann, K. Bothe, J. Schmidt, and R. Brendel, "Permanent deactivation of the boron-oxygen recombination center in silicon solar cells," in *Proc. 23rd Eur. Photovolt. Sol. Energy Conf.*, Valencia, Spain, 2008, pp. 1018–1022.
- [42] J. Knobloch *et al.*, "21% efficient solar cells processed from Czochralski grown silicon," in *Proc. 13th Eur. Photovolt. Sol. Energy Conf.*, 1995, pp. 9–12.
- [43] A. Herguth, G. Schubert, M. Käs, and G. Hahn, "A new approach to prevent the negative impact of the metastable defect in boron doped Cz silicon solar cells," in *Proc. 4th IEEE World Conf. Photovolt. Energy Convers.*, vol. 1, 2006, pp. 940–943.
- [44] A. Herguth, G. Hahn, and A. Degradation, "Kinetics of the boron-oxygen related defect in theory and experiment," *J. Appl. Phys.*, vol. 108, no. 11, pp. 1–7, 2010.
- [45] K. Münzer, "Hydrogenated silicon nitride for regeneration of light induced degradation," in *Proc. 24th Eur. Photovolt. Sol. Energy Conf.*, Hamburg, 2009, pp. 1558–1561.
- [46] G. Krugel, W. Wolke, J. Geilker, S. Rein, and R. Preu, "Impact of hydrogen concentration on the regeneration of light induced degradation," *Energy Proc.*, vol. 8, pp. 47–51, 2011.
- [47] S. Dubois *et al.*, "The BOLID project: Suppression of the boron-oxygen related light-induced-degradation," in *Proc. 27th Eur. Photovolt. Sol. Energy Conf.*, Frankfurt, Germany, 2012, pp. 749–754.
- [48] S. Wilking, A. Herguth, and G. Hahn, "Influence of hydrogen on the regeneration of boron-oxygen related defects in crystalline silicon," *J. Appl. Phys.*, vol. 113, no. 19, 2013.
- [49] B. Hallam *et al.*, "Hydrogen passivation of B-O defects in Czochralski silicon," *Energy Procedia*, vol. 38, pp. 561–570, 2013.
- [50] N. Nampalli, B. Hallam, C. Chan, M. Abbott, and S. Wenham, "Evidence for the role of hydrogen in the stabilization of minority carrier lifetime in boron-doped Czochralski silicon," *Appl. Phys. Lett.*, vol. 106, no. 17, p. 173501, 2015.
- [51] S. R. Wenham *et al.*, "Advanced hydrogenation of silicon solar cells," WO2013173867A1, 2013.
- [52] S. Wilking, C. Beckh, S. Ebert, A. Herguth, and G. Hahn, "Influence of bound hydrogen states on BO-regeneration kinetics and consequences for high-speed regeneration processes," *Sol. Energy Mater. Sol. Cells*, vol. 131, pp. 2–8, 2014.
- [53] P. Hamer, B. Hallam, M. Abbott, and S. Wenham, "Accelerated formation of the boron-oxygen complex in p-type Czochralski silicon," *Phys. Status Solidi - Rapid Res. Lett.*, vol. 9, no. 5, pp. 297–300, 2015.
- [54] B. J. Hallam *et al.*, "Rapid mitigation of carrier-induced degradation in commercial silicon solar cells," *Jpn. J. Appl. Phys.*, vol. 56, no. 8S2, p. 08MB13, 2017.
- [55] D. Walter, T. Pernau, and J. Schmidt, "Ultrafast lifetime regeneration in an industrial belt-line furnace applying intense illumination at elevated temperature," in *Proc. 32nd Eur. Photovolt. Sol. Energy Conf. Exhib.*, Jul. 2016, pp. 469–473.
- [56] B. Hallam *et al.*, "Modelling the long-term behaviour of boron-oxygen defect passivation in the field using typical meteorological year data (TMY2)," in *Proc. 32nd Eur. Photovolt. Sol. Energy Conf. Exhib.*, vol. 1, 2016, pp. 555–559.
- [57] B. Hallam *et al.*, "Modelling kinetics of the boron-oxygen defect system," *Energy Proc.*, vol. 92, pp. 42–51, 2016.
- [58] W. De Soto, "Improvement and validation of a model for photovoltaic array performance," M.S. thesis, Univ. Wisconsin-Madison, 2004.
- [59] W. De Soto, S. A. Klein, and W. A. Beckman, "Improvement and validation of a model for photovoltaic array performance," *Sol. Energy*, vol. 80, no. 1, pp. 78–88, 2006.
- [60] T. Neises, "Development and validation of a model to predict the cell temperature of a photovoltaic cell," M.S. thesis, Solar Energy Laboratory as part of the college of Engineering, Univ. Wisconsin-Madison, 2011.
- [61] Meteotest, "Meteonorm v5.0.13," Bern, Switzerland, 2003.
- [62] K. Lee *et al.*, "Natural recovery from LID: Regeneration under field conditions?" in *Proc. 31st Eur. Photovolt. Sol. Energy Conf. Exhib.*, 2015, pp. 1835–1837.
- [63] S. Wilking, M. Forster, A. Herguth, and G. Hahn, "From simulation to experiment: Understanding BO-regeneration kinetics," *Sol. Energy Mater. Sol. Cells*, vol. 142, pp. 87–91, 2015.
- [64] B. J. Hallam, M. Abbott, N. Nampalli, P. G. Hamer, and S. R. Wenham, "Implications of accelerated recombination-active defect complex formation for mitigating carrier-induced degradation in silicon," *IEEE J. Photovolt.*, vol. 6, no. 1, pp. 92–99, Jan. 2016.
- [65] B. Hallam, M. Abbott, N. Nampalli, P. Hamer, and S. Wenham, "Influence of the formation- and passivation rate of boron-oxygen defects for mitigating carrier-induced degradation in silicon within a hydrogen-based model," *J. Appl. Phys.*, vol. 119, p. 65701, 2016.
- [66] A. Herguth and B. Hallam, "A generalized model for boron-oxygen related light-induced degradation in crystalline silicon," *AIP Conf. Proc.*, vol. 1999, Aug. 2018, pp. 1–5.
- [67] V. V. Voronkov and R. Falster, "Latent complexes of interstitial boron and oxygen dimers as a reason for degradation of silicon-based solar cells," *J. Appl. Phys.*, vol. 107, no. 5, p. 53509, Mar. 2010.
- [68] B. Hallam *et al.*, "Rapid processing of boron-oxygen defects," in *Proc. 31st Eur. PVSEC*, 2015, pp. 531–535.

- [69] A. Herguth, G. Schubert, M. Käs, G. Hahn, and I. Melnyk, "Method for fabricating a photovoltaic element with stabilised efficiency," WO2007107351A1, 2012.
- [70] D. C. Walter and J. Schmidt, "Impact of hydrogen on the permanent deactivation of the boron-oxygen-related recombination center in crystalline silicon," *Sol. Energy Mater. Sol. Cells*, vol. 158, pp. 91–97, 2016.
- [71] H. Hashigami, Y. Itakura, and T. Saitoh, "Effect of illumination conditions on Czochralski-grown silicon solar cell degradation," *J. Appl. Phys.*, vol. 93, no. 7, pp. 4240–4245, 2003.
- [72] V. V. Voronkov, R. J. Falster, J. Schmidt, K. Bothe, and A. Batunina, "(Invited) lifetime degradation in boron doped Czochralski silicon," *ECS Trans.*, vol. 33, no. 11, pp. 103–112, 2010.
- [73] T. U. Nærland, H. Angelskår, and E. S. Marstein, "Direct monitoring of minority carrier density during light induced degradation in Czochralski silicon by photoluminescence imaging," *J. Appl. Phys.*, vol. 113, no. 19, p. 193707, 2013.
- [74] A. Herguth, G. Schubert, M. Käs, and G. Hahn, "Investigations on the long time behavior of the metastable boron-oxygen complex in crystalline silicon," *Prog. Photovolt. Res. Appl.*, vol. 16, no. 2, pp. 135–140, 2008.
- [75] L. Helmich *et al.*, "In-situ characterization of electron-assisted regeneration of Cz-Si solar cells," *Sol. Energy Mater. Sol. Cells*, vol. 185, pp. 283–286, 2018.
- [76] S. Wilking, S. Ebert, A. Herguth, and G. Hahn, "Influence of hydrogen effusion from hydrogenated silicon nitride layers on the regeneration of boron-oxygen related defects in crystalline silicon," *J. Appl. Phys.*, vol. 114, no. 19, p. 194512, Nov. 2013.
- [77] K. Bothe and J. Schmidt, "Electronically activated boron-oxygen-related recombination centers in crystalline silicon," *J. Appl. Phys.*, vol. 99, no. 1, p. 13701, 2006.
- [78] National Centre for Atmospheric Research Staff, *The Climate Data Guide: Global surface temperatures: BEST: Berkeley Earth Surface Temperatures*. 2014.
- [79] R. Rohde *et al.*, "A new estimate of the average Earth surface land temperature spanning 1753 to 2011," *Geoinform. Geostatist. Overv.*, vol. 1, no. 1, p. 2, 2013.
- [80] R. Rohde *et al.*, "Berkeley earth temperature averaging process," *Geoinform. Geostatist. Overv.*, vol. 1, no. 2, pp. 1–13, 2013.
- [81] N. Cahill, S. Rahmstorf, and A. C. Parnell, "Change points of global temperature," *Environ. Res. Lett.*, vol. 10, no. 8, p. 084002, 2015.
- [82] J. E. Overland *et al.*, "Nonlinear response of mid-latitude weather to the changing Arctic," *Nat. Clim. Chang.*, vol. 6, p. 992, Oct. 2016.
- [83] F. Fertig *et al.*, "Mass production of p-type Cz silicon solar cells approaching average stable conversion efficiencies of 22%," *Energy Proc.*, vol. 124, 2017, pp. 338–345.
- [84] B. Sopori *et al.*, "A comprehensive model of hydrogen transport into a solar cell during silicon nitride processing for fire-through metallization," in *Proc. Conf. Rec. 31st IEEE Photovolt. Spec. Conf.*, Feb. 2005, pp. 1039–1042.
- [85] S. De Wolf *et al.*, "High-efficiency silicon heterojunction solar cells: A review," *Green*, vol. 2, no. 1, pp. 7–24, Jan. 2012.
- [86] A. Ciesla *et al.*, "High-voltage p-type PERC solar cells with anchored plating and hydrogenation," *Prog. Photovolt. Res. Appl.*, pp. 397–401, 2018.
- [87] F. Kersten *et al.*, "A new mc-Si degradation effect called LeTID," in *Proc. 42nd IEEE Photovolt. Spec. Conf.*, 2015, pp. 1–5.
- [88] A. Ciesla *et al.*, "Hydrogen-induced degradation," in *Proc. 7th World Conf. Photovolt. Energy Convers. (WCPEC)*, 2018, pp. 1–8.
- [89] M. A. Jensen *et al.*, "Evaluating root cause: The distinct roles of hydrogen and firing in activating light- and elevated temperature-induced degradation," *J. Appl. Phys.*, vol. 124, no. 8, p. 85701, Aug. 2018.
- [90] D. Bredemeier, D. C. Walter, and J. Schmidt, "Lifetime degradation in multicrystalline silicon under illumination at elevated temperature: Indications for the involvement of hydrogen," in *AIP Conf. Proc.*, vol. 1999, no. 1, Aug. 2018, p. 130001.
- [91] D. Chen *et al.*, "Hydrogen induced degradation: A possible mechanism for light- and elevated temperature-induced degradation in n-type silicon," *Sol. Energy Mater. Sol. Cells*, vol. 185, pp. 174–182, 2018.
- [92] T. H. Fung *et al.*, "Influence of bound hydrogen states on carrier-induced degradation in multi-crystalline silicon," in *AIP Conf. Proc.*, vol. 1999, no. 1, Aug. 2018, p. 130004.
- [93] C. Vargas *et al.*, "Carrier-induced degradation in multicrystalline silicon: dependence on the silicon nitride passivation layer and hydrogen released during firing," *IEEE J. Photovolt.*, vol. 8, no. 2, pp. 413–420, Mar. 2018.
- [94] T. Niewelt *et al.*, "Understanding the light-induced degradation at elevated temperatures: Similarities between multicrystalline and floatzone p-type silicon," *Prog. Photovolt. Res. Appl.*, vol. 26, no. 8, pp. 533–542, Aug. 2018.